Langmuir

Article

pubs.acs.org/Langmuir

Highly Sensitive Visual Detection of Copper Ions Based on the Shape-Dependent LSPR Spectroscopy of Gold Nanorods

Zhiyang Zhang,[†,‡,§] Zhaopeng Chen,*[,†,‡] Chengli Qu,[†,‡] and Lingxin Chen*[,†,‡]

[†]Key Laboratory of Coastal Environmental Processes and Ecological Remediation, Yantai Institute of Coastal Zone Research (YIC), Chinese Academy of Sciences(CAS) and [‡]Shandong Provincial Key Laboratory of Coastal Environmental Processes, YICCAS, Yantai Shandong 264003, P. R. China

[§]University of Chinese Academy of Sciences, Beijing 100049, China

Supporting Information

ABSTRACT: We have developed a novel approach to the rapid visual detection of Cu^{2+} in natural samples based on the copper-mediated leaching of gold nanorods (GNRs). In the presence of hexadecyltrimethylammonium bromide, which can reduce the redox potential of Au(I)/Au, the GNRs are catalytically etched by Cu^{2+} preferentially along the longitudinal direction. And as a result, the localized surface plasmon resonance extinction peak shifts to short wavelength, accompanied by a color change from blue to red. The leaching mechanism has been carefully discussed in a series of control experiments. Under optimal conditions, this sensor exhibits good sensitivity (LOD = 0.5 nM). Most importantly, the approach is highlighted by its high selectivity for and tolerance of interference, which enables the sensor to detect Cu^{2+} directly in a complex matrix, especially in seawater. Moreover, such a nanoparticle-based sensor is also successfully applied to test paper for the visual detection of Cu^{2+}.

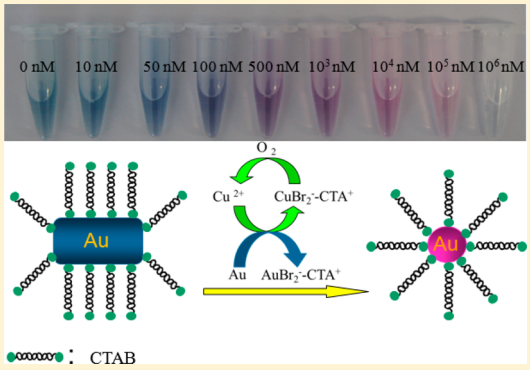

INTRODUCTION

Since the exposure of the Minamata event in the 1950s, contamination by heavy metals has aroused extensive public concern. The risk of such pollutants, even at "invisible" trace levels in the environment, is that they can be progressively concentrated through the food chain and present a threat to human health.[1] Among heavy metals, despite its less-significant toxicity, copper has become a widely distributed pollutant in natural water as a result of the dumping of electronic trash and mining residues. The rapid onsite monitoring of Cu^{2+} is thereby emerging as an important analytic issue.[2] However, the strong dependence of developed methods on instruments (AAS, AES, ICP-MS, etc.) prevents them from being used in outside-laboratory applications. Such methods would also be affected by the complex matrix of certain natural waters (e.g., the matrix effects of seawater on ICP-MS[3] and the interference of organics in anodic/cathodic stripping voltammetry[4−6]). The development of a portable but highly sensitive and selective method is thus urgently needed. To realize this purpose, many quantum-dot-based fluorescent probes have been designed for Cu^{2+}.[7−11] Such probes, compared to traditional organic probes, yield better sensitivity and selectivity but suffer from the interference of the sample matrix and the time-consuming process of the preparation of these functionalized quantum dots. A visual method based on the Cu^{+}-dependent click reaction,[2] showing high selectivity and tolerance to interference, has a relative high detection limit (3.0 μM), which limits its application in most cases. Colorimetric probes based on target-inducing nanoparticle aggregation, compared to traditional chromogenic reagent-based methods, have proven to be more sensitive. These probes still encounter difficulties in sensing Cu^{2+} in complex matrixes because of the autoaggregation in water samples.[12−15]

Recently, a promising new strategy for sensing metal ions (Pb^{2+}) based on the catalytic etching of gold nanoparticles was first developed by Chen et al.[16] The formation of a PbAu alloy decreased the redox potential of Au(I)/Au(0). In the presence of thiosulfate and mercaptoethanol, gold nanoparticles were oxidized by dissolved oxygen to produce Au(I). The wine-red colloidal gold was therefore bleached. Thereafter, our group developed similar methods for sensing Cu(II).[17,18] With the presence of thiosulfate, gold or silver nanoparticles were oxidized by Cu(II) to produce Au(I) or Ag(I) and Cu(I). The latter was then oxidized by dissolved oxygen, and Cu(II) was regenerated. The circle also led to the bleaching of colloidal gold or silver. Although these methods are sensitive and can be applied to the sensing of Cu(II) in tap water and drinking water, the low stability of thiosulfate-stabilized nanoparticles limited their application in complex matrixes. For example, high salt in seawater would lead to the aggregation of these nanoparticles.

In this work, using cetyltrimethylammonium bromide (CTAB)-stabilized gold nanorods (GNRs), the color of which is dependent on the aspect ratio,[19,20] we have proposed a simple

Received: January 9, 2014
Revised: March 9, 2014
Published: March 11, 2014

   dx.doi.org/10.1021/la500106a | *Langmuir* 2014, 30, 3625−3630

and sensitive visual sensor for Cu^{2+} based on the catalytic etching of GNRs. In this system, CTAB acts not only as a stabilizer but also as an ion-association reagent. As an association reagent, CTAB reduces the redox potential of Au(I)/Au(0), allowing GNRs to be oxidized by Cu^{2+}. Additionally, the high binding force between the amino group of CTAB and gold could keep GNRs stable in a complex matrix. Thus a visual sensor can be used for the sensing of Cu^{2+} in a complex matrix, such as lake water, digested shellfish samples, and especially seawater.

EXPERIMENTAL SECTION

Chemicals and Apparatus. Hydrogen tetrachloroaurate(III) dehydrate, sodium borohydride, ascorbic acid, hydrochloric acid, silver nitrate, cetyltrimethylammonium bromide (CTAB), and $CuSO_4$ were obtained from Sinopharm Chemical Reagent (China). All other chemicals were analytical reagent grade or better. Solutions were prepared with deionized water (18.2 MΩ, Pall Cascada). Filter paper (Supor 450, 0.45 μm) was obtained from the Pull Corporation of America.

Transmission electron microscopy (TEM) analyses were performed on a JEM-1230 electron microscope (Japan) operating at 100 kV. Extinction spectra were recorded on a Thermo Scientific NanoDrop 2000/2000C spectrophotometer.

Preparation of Gold Nanorods. Gold nanorods with different aspects (length/width ratio) were synthesized according to a modified method by changing the amount of $AgNO_3$.[21] The obtained gold nanorods were centrifuged twice at 8000 rpm for 15 min to remove excess ascorbic acid that would inhibit the sensitivity of the proposed probe (Supporting Information, Figure S1). The obtained soft sediment was then resuspended in deionized water. Finally, a different amount of CTAB was added to the gold nanorod solution.

Procedure for Sensing Cu^{2+}. The prepared gold nanorods (200 μL) were added to a hydrogen bromide-adjusted buffer solution (800 μL, 0.5 M) containing different concentrations of Cu^{2+} ions. The final concentration of gold nanorods was calculated to be about 0.33 nM.[22] After incubation at 75 °C for 20 min, the resulting solution was then subjected to UV−vis spectroscopic measurements.

RESULTS AND DISCUSSION

Scheme 1 presents the sensing mechanism for the detection of Cu^{2+}. In the absence of Cu^{2+}, CTAB-stabilized GNRs were

Scheme 1. Schematic Illustration of the Sensing Mechanism for the Detection of Cu^{2+}

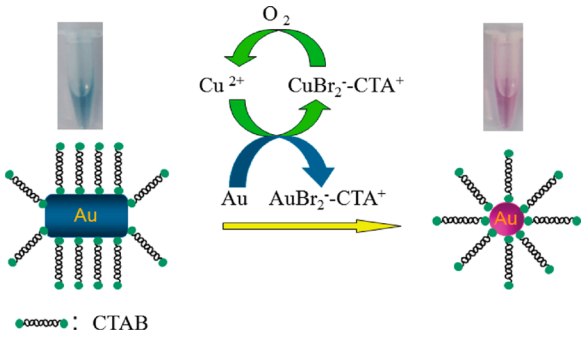

etched slowly by dissolved oxygen in hydrobromic acid solution[23] and the GNR solution remained blue during the incubation process (20 min). The negligible color change corresponds well to the slight change in the localized surface plasmon resonance (LSPR) extinction spectrum of GNRs (Supporting Information, Figure S2). With addition of Cu^{2+}, the GNRs were catalytically etched along the longitudinal direction (Supporting Information, Figure S3). The etching of GNRs resulted in the decrease of aspect ratio of GNRs as shown in the TEM images (Figure 1) and the aspect ratio distributions

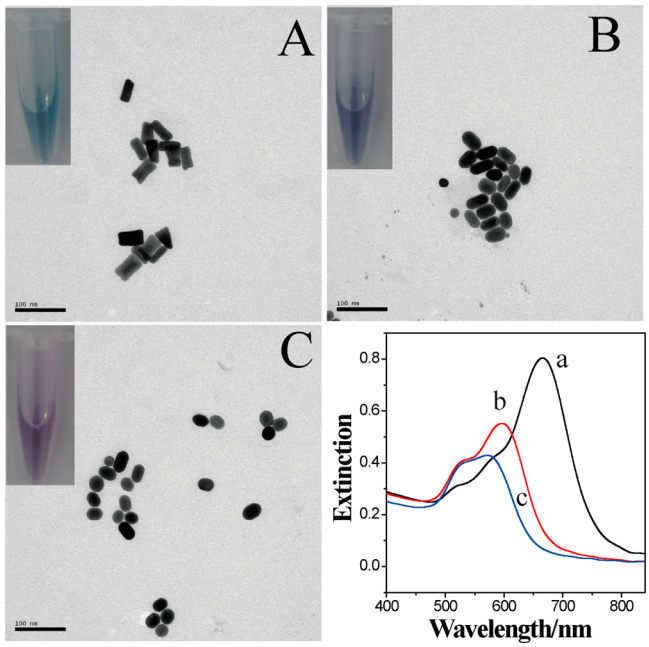

Figure 1. TEM images and extinction spectra of GNRs after incubation with 0 (A, a), 1.0 (B, b), and 10 μM Cu^{2+} (C, c) in 0.5 M HBr at 75 °C for 20 min.

(Figure S3, Supporting Information). The preferential shortening along the longitudinal direction can be attributed to less surface passivation and/or higher reaction activities at the tips of the gold nanorods.[23−25] The anisotropic etching led to the blue shift of the LSPR extinction spectrum of GNRs (Figure 1), accompanied by a color change from blue to red and even to colorless with the increase in Cu^{2+}, providing a visual method for sensing Cu^{2+} (Scheme 1).

To explore the etching mechanism, we added a high concentration of Cu^{2+} (2 mM) to the colloidal gold in the presence of 0.5 M HBr, and the solution was incubated at room temperature for several minutes. The color of the mixture changed to colorless within 5 min (Figure S4, Supporting Information). This indicated that Au was transformed to Au(I) instead of Au(III). In addition, a new absorption band at around 280 nm was immediately obtained as the colloid turned colorless. As the incubation progressed, the absorption at 280 nm decreased gradually with time, suggesting the formation of Cu(I) and the further transformation of Cu(I) to other species (Figure S5, Supporting Information).[26]

Judging from the redox potential of $AuBr_2^-$/Au (0.93 V vs the normal hydrogen electrode, NHE) and $Cu^{2+}/CuBr_2^+$ (0.52 V vs NHE), theoretically gold cannot be oxidized by Cu^{2+}. The etching of GNRs by Cu^{2+} in this study, we think, should be related to the conjugation of CTA^+ with $CuBr_2^+$ and $AuBr_2^-$. Figure S6 in the Supporting Information illustrates the effect of CTAB on the etching of wine-red gold nanoparticles (13 nm). Herein we used AuNPs to replace GNRs because the synthesis of AuNPs needs no introduction of CTAB. Prepared AuNPs were first stabilized by 0.4% tween-20 in 0.5 HBr solution. Without or with the addition of Cu^{2+}, the color of the AuNP solutions remained wine red, and the extinction peak around 520 nm was not altered, indicating no etching of AuNPs occurred. Thereafter,

dx.doi.org/10.1021/la500106a | Langmuir 2014, 30, 3625−3630

2 mM CTAB was introduced, and the color changed to reddish with a decrease in the extinction peak at around 520 nm. It was also observed that the etching rate would be improved with the increase in CTAB concentration. To confirm that the etching process was essentially affected by CTA^+ but not by increasing the Br^- concentration, a control experiment was also conducted by replacing CTAB with NaBr. As shown in Figure S7 in the Supporting Information, different concentrations of NaBr of less than 4 mM had little effect on the etching of tween-20-stabilized gold nanoparticles.

In the presence of CTA^+, the redox potential of $AuBr_2^-$−CTA^+/Au, $E_{AuBr_2^-CTA^+/Au}$ could decline to less than 0.2 V (vs NHE).[27] In contrast, $E_{Cu^{2+}/CuBr_2^-}$ is 0.52 V (vs NHE), and we can conclude that this value will be higher than 0.52 V (vs NHE) because $CuBr_2^-$ can also conjugate with CTA^+. Theoretically, Au can be oxidized by Cu^{2+} to produce $AuBr_2^-$−CTA^+ and $CuBr_2^-$−CTA^+. In addition, E_{O_2/H_2O} is about 1.20 V (vs NHE) in acid solution calculated according to the Nernst equation. Therefore, the following circle was thereby presumed for the continuous etching of GNRs:

$$Au + Cu^{2+} + CTA^+ + Br^- \rightarrow AuBr_2^-{-}CTA^+ + CuBr_2^-{-}CTA^+$$

$$CuBr_2^-{-}CTA^+ + O_2 \rightarrow Cu^{2+} + H_2O + Br^- + CTA^+$$

To test this assumption, several control experiments were conducted from different aspects. Figure 2 describes the effect of

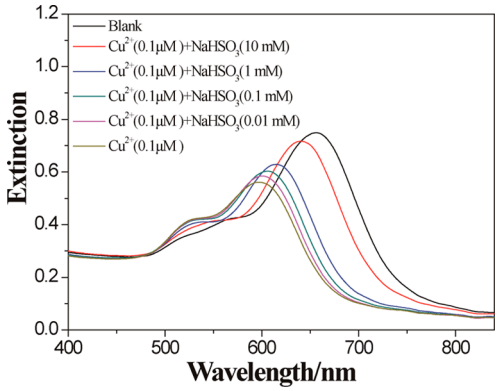

Figure 2. Extinction spectra of GNRs after incubation with 0.1 μM Cu^{2+} in 0.5 M HBr after removing dissolved oxygen by the addition of different concentrations of $NaHSO_3$ at 75 °C for 20 min.

dissolved oxygen on the etching process. It was observed that, with the preremoval of dissolved oxygen by the addition of $NaHSO_3$ ($2SO_3^{2-} + O_2 \rightarrow 2SO_4^{2-}$), the etching of GNRs was inhibited by the less-significant blue shift. Moreover, the etching rate decreased with the increasing $NaHSO_3$ concentration. These results indicated that dissolved oxygen participated in the etching reaction and may oxidize $CuBr_2^-$−CTA^+ to Cu^{2+}.

Thereafter, an aliquot of 0.1 M CuBr in HBr solution was mixed with an equal volume of 0.1 M CTAB. The mixture immediately changed to a milky-white emulsion, suggesting the formation of $CuBr_2^-$−CTA^+ as an ion-association complex. The emulsion was then incubated at 75 °C for 5 min, and a clear solution was obtained. However, the process would not be reversibly converted when the temperature decreased. This phenomenon should be due to the oxidation of $CuBr_2^-$−CTA^+ by dissolved oxygen, which converted barely soluble $CuBr_2^-$−CTA^+ to highly soluble Cu^{2+}. Figure S8 in the Supporting Information illustrates the absorption spectrum of 1 mM $CuBr_2^-$−CTA^+ after incubation at room temperature for different times (curves a−c). The absorption at around 280 nm was observed to decrease gradually with the increase in incubation time and finally showed no difference to that of 1 mM Cu^{2+} in the presence of CTAB (curve d). Thus, the oxidation of $CuBr_2^-$−CTA^+ by dissolved oxygen could also be verified.

Because $CuBr_2^-$−CTA^+ could be oxidized by dissolved oxygen, it is reasonable to assume that Cu^+ would catalyze the etching of GNRs by dissolved oxygen in HBr solutions in the presence of CTAB. Figure S9 in the Supporting Information demonstrates the test results of such an assumption. A blue shift of the longitudinal LSPR extinction peak was observed. The blue shift appeared to be more significant with the increase in CuBr. It can be concluded that the etching of GNRs by dissolved oxygen could also be accelerated by Cu^+.

Inspired by the outstanding catalytic property of Cu^{2+} upon the etching of GNRs, a simple and practical sensor was used for the sensing of Cu^{2+} in a complex matrix. Several key factors, including the CTAB concentration, temperature, and time were optimized (Figures S10−S15, Supporting Information). Figure 3 shows the responses of the proposed sensors to different concentrations of Cu^{2+} under the optimal condition. The longitudinal LSPR extinction peak of GNRs were bleached and shifted to short wavelength gradually with increasing Cu^{2+} concentration (Figure 3A,B). Two different linear relationships, one between the peak shift and Cu^{2+} concentrations (1.0 to 20 nM, Figure 3C) and the other between the peak shift and logarithm of Cu^{2+} concentrations (20 to 10^5 nM, Figure 3D), were respectively obtained. The detection limit was calculated to be 0.5 nM according to the $S/N = 3$ rule, which is lower than that of other nanoparticles and quantum-dot-based sensors,[7−11,17,18,28] and is comparable to the results obtained by AAS, AES, ICPMS, and anodic/cathodic stripping voltammetry (Table 1).[29−35] Digital photographs (Figure 3E) show that the color of the GNR solutions changed from blue to red and even to colorless with increasing Cu^{2+} content. The color change induced by 50 nM Cu^{2+} can be easily observed by the naked eye. Such a concentration is almost 3 orders of magnitude lower than the safety limit defined by WHO (20 μM).

The specificity of the sensor toward Cu^{2+} was evaluated by examining the extinction spectra of GNRs in HBr solution in the presence of various other cations and anions, including Li^+, Na^+, K^+, Ca^{2+}, Mg^{2+}, Al^{3+}, Zn^{2+}, Fe^{3+}, Pb^{2+}, Hg^{2+}, Ag^+, Mn^{2+}, Co^{2+}, Ni^{2+}, Cd^{2+}, Cr(VI), NO_3^-, SO_4^{2-}, PO_4^{3-}, and NO_2^- at a concentration of 1.0 μM (Figure 4). It was found that the color and spectra of GNRs changed very little with the addition of those ions. However, the addition of 0.1 μM Cu^{2+} caused the solution color to change from blue to blue-gray, accompanied by a significant peak shift in the longitudinal LSPR extinction. A greater concentration of Cu^{2+} (1.0 μM) led to a more obvious color change and more peak shifts. The interference of other ions was also evaluated by mixing the ions mentioned above (each at a concentration of 1.0 μM) and GNRs in HBr solution in the presence and absence of Cu^{2+}. The results showed that the presence of those ions had negligible effects on the detection of Cu^{2+}. For these reasons, we concluded that the probe displayed excellent selectivity toward Cu^{2+}.

To test the applicability of the proposed probe for Cu^{2+} detection in real samples, several samples including lake water (Sanyuan lake, Yantai university), seawater (certified seawater purchased from National Research Council Canada), and

dx.doi.org/10.1021/la500106a | Langmuir 2014, 30, 3625−3630

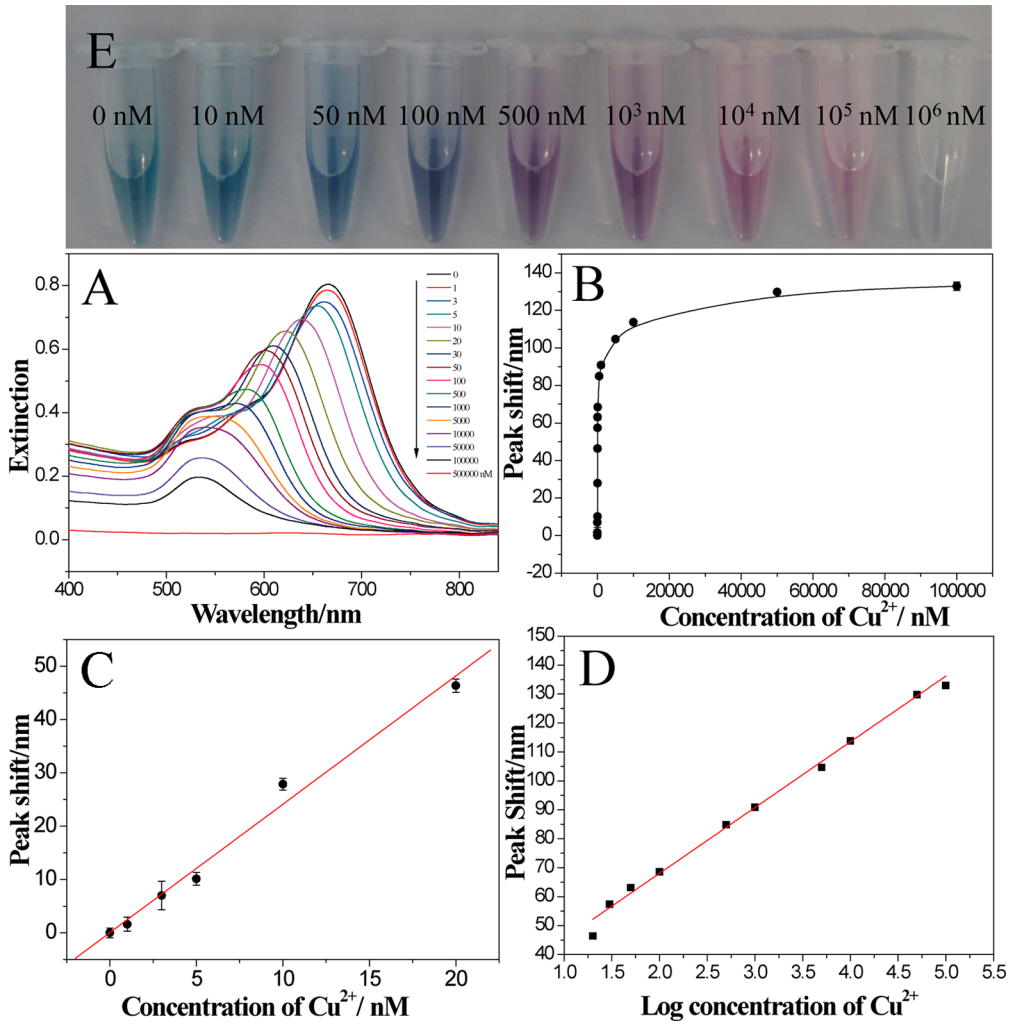

Figure 3. Extinction spectra (A), longitudinal LSPR extinction peak shifts (B–D), and color changes (E) of GNRs after incubation with different concentrations of Cu^{2+}.

Table 1. Comparison of the Performance of Different Analytical Methods for the Detection of Cu^{2+}

material/method	detection limit	sample	ref
hybrid material composed of SiO_2, Al_2O_3, and TiO_2/AAS	0.5 ppb	tap and mineral water and ethanol fuel	29
Amberlite XAD-2-functionalized 3-(2-nitropheny1)-1*H*-1,2,4-triazole-5(4*H*)-thione/AES	0.18 ppt	river water and vegetables	30
chitosan-grafted multiwalled carbon nanotubes/ICPMS	3.5 ppt	herring, spinach, and river and tap water	31
gold nanoelectrode ensembles/voltammetry	subppb		32
gold microwire electrode/voltammetry	25 pM	coastal water	33
gold cysteamine self-assembled monolayer functionalized with salicylaldehyde/voltammetry	75 pM	blood serum and synthetic sample	34
cysteine-modified gold electrode/voltammetry	0.39 nM	river and seawater	35
16-mercaptohexadecanoic acid-capped CdSe QDs/fluorescence	5 nM	physiological fluids	8
polyamine-functionalized carbon quantum dots/fluorescence	6 nM	river water	7
polyethylenimine-protected silver nanoclusters/fluorescence	10 nM	river, lake, tap, and spring water	11
meso-2,3-dimercaptosuccinic acid DMSA-capped CdTe QDs/visual detection	10 nM	synthetic sample	9
(sodium poly(2-(4-methyl-3-thienyloxy)propanesulfonate/click-reaction-based visual detection	3 μM	tap and lake water	2
thiosulfate-stabilized Ag/Au nanoparticles/visual detection/visual and spectrophotometric detection	~50 nM/1 nM	tap and pond water	17
CTAB-stabilized gold nanoparticles/visual and spectrophotometric detection	40 nM/5.0 nM	shellfish, tap and drinking water	18
azide- and alkyne-functionalized gold nanoparticles/click-reaction-based visual detection	50 μM		28
CTAB-stabilized gold nanorods/visual and spectrophotometric detection	50 nM/0.5 nM	shellfish, lake and seawater	this work

digested shellfish samples were tested using this probe. Table 2 shows the detection results using the proposed probe. The detection results are consistent with the certified concentration, spiked concentrations, and ICPMS results. It is particularly noteworthy that our sensor yields excellent tolerance to the high salinity of seawater without any aggregation during the etching

dx.doi.org/10.1021/la500106a | *Langmuir* 2014, 30, 3625–3630

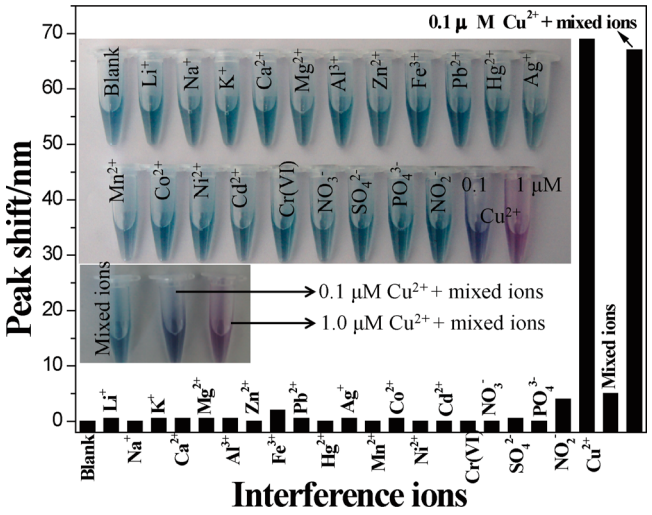

Figure 4. LSPR extinction peak shift and color change (photograph inset) of GNRs after incubation with various environmental ions. [Cu^{2+}] = 0.1 μM, [other ions] = 1.0 μM.

Table 2. Determination Results in Real Samples by the Proposed Method

sample		certified or spiked concentration	detected	recovery (%)	relative error (%)
digested shellfish samples	sample 1	8.6 μM[a]	9.2 μM	106.9	4.1
	sample 2	14.4 μM[a]	12.6 μM	88.2	12.3
	sample 3	12.2 μM[a]	14.7 μM	120.4	3.5
	sample 4	14.3 μM[a]	12.6 μM	88.1	4.1
	sample 5	10.6 μM[a]	11.9 μM	111.5	3.5
lake water	sample 1	0.5 μM[b]	5.9 μM	119.1	11.1
	sample 2	1.0 μM[b]	10.7 μM	107.3	6.5
	sample 3	1.5 μM[b]	1.38 μM	91.7	4.1
seawater	sample 1	0.371 ppb[c]	0.395 ppb	106.4	15.5
	sample 2	5 ppb[b]	4.63 ppb	92.6	4.3
	sample 3	100 ppb[b]	87.4 ppb	87.4	2.1

[a]ICPMS results. [b]Spiked concentrations. [c]Certified concentration.

process (Figures S16 and S17, Supporting Information), which is why this method can be used in seawater. For a long time, the detection of trace metals in seawater has been a forbidden subject for nanoparticles-based visual probes. Such results demonstrate that our probe could be a practical tool for the rapid on-site monitoring of Cu^{2+} (especially in seawater).

On the basis of the above efforts, a simple test paper was also preliminarily developed for the visual detection of Cu^{2+}. Briefly, 5.0 μL of a CTAB-stabilized GNR colloid was dropped onto a specific zone of filter papers (Supor 450, 0.45 μm, Pall Corporation, USA). The solution was thereafter evaporated in air sufficiently. The sensing zone was immersed in a 2 M HBr solution premixed with target or standard aqueous samples. After incubation at 75 °C for 20 min, the color of each test zone was inspected and compared. The color turned red and even colorless gradually wit increasing Cu^{2+} content (Figure 5), which is obvious enough to the naked eye at a concentration of 100 nM. The recognizable limit of such a test paper, as tested by uninformed volunteers, was 100 nM for Cu^{2+} with the naked eye. The designed test paper, as compared to other reports, is much simpler, more economical, and more practical for the detection of Cu^{2+}.[36−38]

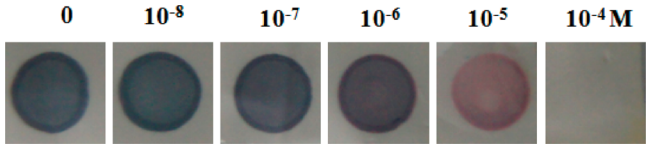

Figure 5. Photographs of the proposed test paper for the sensing of different concentrations of Cu^{2+}.

CONCLUSIONS

We have developed a novel approach for the visual sensing of Cu^{2+} with high sensitivity and selectivity in aqueous media based on the catalytic etching of GNRs, which caused a change in the shape-dependent LSPR spectroscopy of GNRs. Compared to other sensors for the detection of Cu^{2+}, our sensor shows a rapid response and sensitivity toward Cu^{2+}, with a detectable range (50 nM−1.0 mM) over 5 orders of magnitude by the naked eye. To the best of our knowledge, the visual detection limit, 50 nM, is among the lowest reported for the detection of Cu^{2+}. Importantly, this sensor is highlighted by its excellent selectivity and high tolerance to interference, which enables the sensor to detect Cu^{2+} directly in a complex matrix without complicated processes of sample pretreatment. Because the approach avoids the need for sophisticated equipment, the sensor promises to be a practical tool for the in situ monitoring of Cu^{2+}. Moreover, such a nanoparticle-based sensor is applied to test paper for the detection Cu^{2+} with the naked eye. The test paper would be potentially used in the rapid detection of Cu^{2+} in real samples.

ASSOCIATED CONTENT

Supporting Information

UV−vis extinction/absorption spectra; photographs of $HAuCl_4$(III), Au(I), GNRs with different aspect ratios; and GNR distributions for the proposed proof of mechanism. This material is available free of charge via the Internet at http://pubs.acs.org.

AUTHOR INFORMATION

Corresponding Authors

*E-mail zhpchen@yic.ac.cn. Fax/phone: 086-535-2109133.
*E-mail lxchen@yic.ac.cn. Fax/phone: 086-535-2109130.

Notes

The authors declare no competing financial interest.

ACKNOWLEDGMENTS

This research was financially supported by the Department of Science and Technology of Shandong Province (BS2009DX006), the NSFC (No. 21275158), and the project sponsored by SRF for ROCS and the 100 Talents Program of the CAS.

REFERENCES

(1) Onyido, I.; Norris, A. R.; Buncel, E. Biomolecule–mercury interactions: modalities of DNA base–mercury binding mechanisms. Remediation strategies. *Chem. Rev.* **2004**, *104*, 5911−5929.

(2) Yao, Z. Y.; Yang, Y. B.; Chen, X. L.; Hu, X. P.; Zhang, L.; Liu, L.; Zhao, Y. L.; Wu, H. C. Visual detection of copper(II) ions based on an anionic polythiophene derivative using click chemistry. *Anal. Chem.* **2013**, *85*, 5650−5653.

(3) Leonhard, P.; Pepelnik, R.; Prange, A.; Yamada, N.; Yamada, T. Analysis of diluted sea-water at the ng L^{-1} level using an ICP-MS with an octopole reaction cell. *J. Anal. Atom. Spectrom.* **2002**, *17*, 189−196.

(4) Turyan, I.; Mandler, D. Electrochemical determination of trace amounts of gold(III) by anodic-stripping voltammetry using a chemically-modified electrode. *Anal. Chem.* **1993**, *65*, 2089−2092.

(5) Turyan, I.; Mandler, D. Selective determination of Cr(VI) by a self-assembled monolayer-based electrode. *Anal. Chem.* **1997**, *69*, 894−897.
(6) Turyan, I.; Mandler, D. Self-assembled monolayers in electroanalytical chemistry - application of ω-mercaptocarboxylic acid monolayers for electrochemical determination of ultralow levels of cadmium(II). *Anal. Chem.* **1994**, *66*, 58−63.
(7) Dong, Y. Q.; Wang, R. X.; Li, G. L.; Chen, C. Q.; Chi, Y. W.; Chen, G. N. Polyamine-functionalized carbon quantum dots as fluorescent probes for selective and sensitive detection of copper ions. *Anal. Chem.* **2012**, *84*, 6220−6224.
(8) Chan, Y. H.; Chen, J. X.; Liu, Q. S.; Wark, S. E.; Son, D. H.; Batteas, J. D. Ultrasensitive copper(II) detection using plasmon-enhanced and photo-brightened luminescence of CdSe quantum dots. *Anal. Chem.* **2010**, *82*, 3671−3678.
(9) Wang, P.; Lei, J.; Su, M.; Liu, Y.; Hao, Q.; Ju, H. Highly efficient visual detection of trace copper(II) and protein by the quantum photoelectric effect. *Anal. Chem.* **2013**, *85*, 8735−8740.
(10) Yao, J. L.; Zhang, K.; Zhu, H. J.; Ma, F.; Sun, M. T.; Yu, H.; Sun, J.; Wang, S. H. Efficient ratiometric fluorescence probe based on dual-emission quantum dots hybrid for on-site determination of copper ions. *Anal. Chem.* **2013**, *85*, 6461−6468.
(11) Yuan, Z.; Cai, N.; Du, Y.; He, Y.; Yeung, E. S. Sensitive and selective detection of copper ions with highly stable polyethyleneimine-protected silver nanoclusters. *Anal. Chem.* **2014**, *86*, 419−426.
(12) Weng, Z. Q.; Wang, H. B.; Vongsvivut, J.; Li, R. Q.; Glushenkov, A. M.; He, J.; Chen, Y.; Barrow, C. J.; Yang, W. R. Self-assembly of core-satellite gold nanoparticles for colorimetric detection of copper ions. *Anal. Chim. Acta* **2013**, *803*, 128−134.
(13) Guo, Y.; Wang, Z.; Qu, W.; Shao, H.; Jiang, X. Colorimetric detection of mercury, lead and copper ions simultaneously using protein-functionalized gold nanoparticles. *Biosens. Bioelectron.* **2011**, *26*, 4064−4069.
(14) Ye, S. Q.; Shi, X. H.; Gu, W.; Zhang, Y. X.; Xian, Y. Z. A colorimetric sensor based on catechol-terminated mixed self-assembled monolayers modified gold nanoparticles for ultrasensitive detections of copper ions. *Analyst* **2012**, *137*, 3365−3371.
(15) Yang, W. R.; Gooding, J. J.; He, Z. C.; Li, Q.; Chen, G. N. Fast colorimetric detection of copper ions using L-cysteine functionalized gold nanoparticles. *J. Nanosci. Nanotechnol.* **2007**, *7*, 712−716.
(16) Chen, Y. Y.; Chang, H. T.; Shiang, Y. C.; Hung, Y. L.; Chiang, C. K.; Huang, C. C. Colorimetric assay for lead ions based on the leaching of gold nanoparticles. *Anal. Chem.* **2009**, *81*, 9433−9439.
(17) Lou, T.; Chen, L.; Chen, Z.; Wang, Y.; Chen, L.; Li, J. Colorimetric detection of trace copper ions based on catalytic leaching of silver-coated gold nanoparticles. *ACS Appl. Mater. Interfaces* **2011**, *3*, 4215−4220.
(18) Liu, R.; Chen, Z.; Wang, S.; Qu, C.; Chen, L.; Wang, Z. Colorimetric sensing of copper(II) based on catalytic etching of gold nanoparticles. *Talanta* **2013**, *112*, 37−42.
(19) Perez-Juste, J.; Liz-Marzan, L. M.; Carnie, S.; Chan, D. Y. C.; Mulvaney, P. Electric-field-directed growth of gold nanorods in aqueous surfactant solutions. *Adv. Funct. Mater.* **2004**, *14*, 571−579.
(20) Chen, H.; Shao, L.; Li, Q.; Wang, J. Gold nanorods and their plasmonic properties. *Chem. Soc. Rev.* **2013**, *42*, 2679−2724.
(21) Sau, T. K.; Murphy, C. J. Seeded high yield synthesis of short Au nanorods in aqueous solution. *Langmuir* **2004**, *20*, 6414−6420.
(22) Orendorff, C. J.; Murphy, C. J. Quantitation of metal content in the silver-assisted growth of gold nanorods. *J. Phys. Chem. B* **2006**, *110*, 3990−3994.
(23) Tsung, C. K.; Kou, X. S.; Shi, Q. H.; Zhang, J. P.; Yeung, M. H.; Wang, J. F.; Stucky, G. D. Selective shortening of single-crystalline gold nanorods by mild oxidation. *J. Am. Chem. Soc.* **2006**, *128*, 5352−5353.
(24) Zou, R. X.; Guo, X.; Yang, J.; Li, D. D.; Peng, F.; Zhang, L.; Wang, H. J.; Yu, H. Selective etching of gold nanorods by ferric chloride at room temperature. *CrystEngComm* **2009**, *11*, 2797−2803.
(25) Ni, W.; Kou, X.; Yang, Z.; Wang, J. Tailoring longitudinal surface plasmon wavelengths, scattering and absorption cross sections of gold nanorods. *ACS Nano* **2008**, *2*, 677−686.
(26) Sugasaka, K.; Fujii, A. Studies on the preparation of cuprous-oxide.VIII. A spectrophotometric study of halogenocopper (I) complexes in aqueous 5 M $NaClO_4$ solutions. *Bull. Chem. Soc. Jpn.* **1980**, *53*, 2514−2519.
(27) Rodriguez-Fernandez, J.; Perez-Juste, J.; Mulvaney, P.; Liz-Marzan, L. M. Spatially-directed oxidation of gold nanoparticles by Au(III)-CTAB complexes. *J. Phys. Chem. B* **2005**, *109*, 14257−14261.
(28) Zhou, Y.; Wang, S.; Zhang, K.; Jiang, X. Visual detection of copper(II) by azide- and alkyne-functionalized gold nanoparticles using click chemistry. *Angew. Chem., Int. Ed.* **2008**, *47*, 7454−7456.
(29) Lima, G. F.; Ohara, M. O.; Clausen, D. N.; Nascimento, D. R.; Ribeiro, E. S.; Segatelli, M. G.; Bezerra, M. A.; Tarley, C. R. T. Flow injection on-line minicolumn preconcentration and determination of trace copper ions using an alumina/titanium oxide grafted silica matrix and FAAS. *Microchim. Acta.* **2012**, *178*, 61−70.
(30) Kumar, B. N.; Ramana, D. K.; Harinath, Y.; Seshaiah, K.; Wang, M. C. Separation and preconcentration of Cd(II), Cu(II), Ni(II), and Pb(II) in water and food samples using Amberlite XAD-2 functionalized with 3-(2-nitrophenyl)-1*H*-1,2,4-triazole-5(4*H*)-thione and determination by inductively coupled plasma-atomic emission spectrometry. *J. Agric. Food. Chem.* **2011**, *59*, 11352−11358.
(31) Dai, B.; Cao, M.; Fang, G.; Liu, B.; Dong, X.; Pan, M.; Wang, S. Schiff base-chitosan grafted multiwalled carbon nanotubes as a novel solid-phase extraction adsorbent for determination of heavy metal by ICP-MS. *J. Hazard. Mater.* **2012**, *219*−*220*, 103−110.
(32) Jena, B. K.; Raj, C. R. Gold nanoelectrode ensembles for the simultaneous electrochemical detection of ultratrace arsenic, mercury, and copper. *Anal. Chem.* **2008**, *80*, 4836−4844.
(33) Salaun, P.; van den Berg, C. M. Voltammetric detection of mercury and copper in seawater using a gold microwire electrode. *Anal. Chem.* **2006**, *78*, 5052−5060.
(34) Shervedani, R. K.; Mozaffari, S. A. Copper(II) nanosensor based on a gold cysteamine self-assembled monolayer functionalized with salicylaldehyde. *Anal. Chem.* **2006**, *78*, 4957−4963.
(35) Liu, A. C.; Chen, D. C.; Lin, C. C.; Chou, H. H.; Chen, C. H. Application of cysteine monolayers for electrochemical determination of sub-ppb copper(II). *Anal. Chem.* **1999**, *71*, 1549−1552.
(36) Cheng, C. M.; Martinez, A. W.; Gong, J.; Mace, C. R.; Phillips, S. T.; Carrilho, E.; Mirica, K. A.; Whitesides, G. M. Paper-based ELISA. *Angew. Chem., Int. Ed.* **2010**, *49*, 4771−4774.
(37) Li, J.; Yao, J.; Zhong, W. Membrane blotting for rapid detection of mercury(II) in water. *Chem. Commun.* **2009**, 4962−4964.
(38) Gu, Z.; Zhao, M.; Sheng, Y.; Bentolila, L. A.; Tang, Y. Detection of mercury ion by infrared fluorescent protein and its hydrogel-based paper assay. *Anal. Chem.* **2011**, *83*, 2324−2329.